Heavy Water Isotope Precipitation in Inland East Antarctica Accompanied by Strong Southern Westerly Winds during the Last Glacial Maximum

K. Kino[1], A. Cauquoin[2], A. Okazaki[3], T. Oki[1], and K. Yoshimura[2]

[1]Department of Civil Engineering, Graduate School of Engineering, the University of Tokyo, Tokyo, Japan

[2]Institute of Industrial Science, the University of Tokyo, Kashiwa, Japan

[3]Hirosaki University, Hirosaki, Japan

Corresponding author: Kanon Kino (kanon@hydra.t.u-tokyo.ac.jp)

Key Points:

- Meridional sea surface temperature gradient in the southern mid-latitudes is an important controller of westerlies strength.
- Strong westerlies enhanced the intrusion of warm and humid air contributing to heavy isotope precipitation in inland East Antarctica.
- Water isotopes in Antarctica can help to constrain the representation of southern westerlies during the LGM.

Abstract

Stable water isotope signals in inland Antarctic ice cores have provided wealth of information about past climates. This study investigated atmospheric circulation processes that influence precipitation isotopes in inland Antarctica associated with atmospheric circulations in the southern mid-latitudes during the Last Glacial Maximum (LGM, ~21 000 year ago). We simulated this climate period using an isotope-enabled atmospheric general circulation model (MIROC5-iso) forced with different sea surface boundary conditions. Our results showed a steepened meridional sea surface temperature gradient in the southern mid-latitudes associated with a strengthening of the southern westerlies. This change in the atmospheric circulation enhanced the intrusion of warm and humid air from low latitudes that contributes to precipitation events, inducing heavy isotope precipitation inland East Antarctica. Our results suggest that the representation of past southern westerlies can be constrained using water isotopic signals in Antarctic ice cores.

Plain Language Summary

Stable water isotopes are widely used to reconstruct the past variations of the Earth's climate, like the temperature in Antarctica during Last Glacial Maximum (LGM) ~21,000 years ago. A major focus has been made on this period by the climate community because the increase of temperature from LGM until now has been the same order of magnitude as the increase of temperature due to current global warming. Using an isotope-enable climate model forced with different sea surface temperatures (SST) and sea ice concentrations (SIC), we show that water vapor with high isotopic content from low latitudes reached inland East Antarctica when the meridional SST gradient was enhanced, going with a strengthening of westerly winds in the southern hemisphere. Our study suggests that the representation of the past southern westerlies can be constrained using water isotopic signals in Antarctic ice cores.

1 Introduction

Ratios of stable isotopes of water, $H_2{}^{16}O$, $H_2{}^{18}O$, and $HD^{16}O$, expressed hereafter in the usual δ notation (i.e., $\delta^{18}O$, with respect to V-SMOW scale; Dansgaard, 1964), are widely used to study past Earth's climate variations. $\delta^{18}O$ values measured from Antarctic ice cores allowed to describe the glacial-interglacial temperature cycles over the past ~800,000 years (Augustin et al., 2004; Jouzel et al., 2007; Dome Fuji Ice Core Project Members, 2017). To reconstruct the mean surface air temperature (SAT) changes in the past, the classical isotopic thermometer assumption can be used. There, observed present-day spatial SAT/$\delta^{18}O$ slope can be used as a surrogate for the temporal slope at a given site (Dahe et al., 1994; Dansgaard, 1964; Lorius et al., 1979; Lorius & Merlivat, 1977; Motoyama, 2005; Satow et al., 1999)

However, determination processes of $\delta^{18}O$ precipitation ($\delta^{18}O_p$) on Antarctica and potential biases in the reconstructed SAT required continued investigations (Buizert et al., 2014, 2021; Cauquoin et al., 2015; Sime et al., 2009; Werner et al., 2016). Potential changes in the inversion layer strength of inland Antarctica (Buizert et al., 2021) and elevation in the Antarctic ice sheet (Werner et al., 2018) during past climates, such as the last glacial maximum (LGM), would contribute to the biases. Besides, several studies for the modern Antarctica pointed out that atmospheric circulations in the southern mid-latitudes could affect $\delta^{18}O_p$ and temporal SAT/$\delta^{18}O$ (Dittmann et al., 2016; Fujita & Abe, 2006; Hirasawa et al., 2000, 2013; Kino et al., 2021; Noone & Simmonds, 2002; Schlosser et al., 2010; 2017; Stenni et al., 2016; Turner et al.,

2019). Field-based studies suggested that inland Antarctic ice core records are biased by daily scale warm oceanic air intrusions, typically associated with blocking events (Fujita & Abe, 2006; Hirasawa et al., 2000, 2013). This assumption is statistically supported by some recent studies on satellite observation and isotope-enabled climate modeling (Dittman et al., 2016; Kino et al., 2021; Schlosser et al., 2017; Servettaz et al., 2020; Turner et al., 2019). Moreover, such daily scale warm oceanic air intrusions could introduce bias to the $\delta^{18}O_p$ in Antarctic ice cores because the ice cores should reflect precipitation-weighted $\delta^{18}O_p$ and not the annual mean (Krinner & Werner, 2003; Sime & Wolff, 2011; Werner et al., 2018). The associations between the atmospheric circulations and Antarctic surface climate depend on regions (Kino et al., 2021; Marshall et al., 2017; Marshall & Thompson, 2016) and could differ in past climates.

The atmospheric circulations in the southern mid-latitudes, typically the southern westerlies, are associated with sea surface conditions in the southern mid-latitudes in the present (Nakamura et al., 2008) and LGM (Sime et al., 2013; 2016) climates. LGM, one of the extremely cold climates, is characterized by a low atmospheric CO_2 level (approximately 180 ppm) and highly extended ice sheets in the northern hemisphere (NH) (Kageyama et al., 2021). Despite multiple studies on oceanic and continental sediments and climate model simulations, led by the Paleoclimate Modeling Intercomparison Project (PMIP) (Braconnot et al., 2021; Joussaume & Taylor, 2021), have reconstructed the LGM, there are still considerable uncertainties. The latest version of a gridded climatological reconstruction of sea surface temperatures (SST) and sea ice concentrations (SIC) suggested that the cooling during LGM was moderate, compared to the previous estimations (Paul et al., 2021). Still, it did not consider the ocean dynamics (Paul et al., 2021) and disagreed with proxies that suggested the weak Atlantic meridional ocean circulation (AMOC) during LGM (e.g., McManus et al., 2004).

In this study, we applied two recent sets of sea surface reconstructions (Paul et al., 2021; Sherriff-Tadano et al., accepted) as boundary conditions for an isotope-enabled atmospheric general circulation model (AGCM) to consider uncertainties in the LGM climate related to sea surface conditions, in terms of sea surface cooling and sea ice extension. It enables us to comprehensively investigate the influence of three-dimensional atmospheric circulation on the Antarctic $\delta^{18}O_p$. The remainder of this paper is organized as follows. Section 2 discusses the model, experimental settings, observational dataset, and analysis method. Section 3 presents an evaluation of the simulated LGM climate in Antarctica. Section 4 describes the processes ruling the $\delta^{18}O_p$ in Antarctica by investigating the differences between the simulated LGM experiments. Further discussion and conclusions are presented in Section 5.

2 Materials and Methods

2.1 Isotope-enabled atmospheric general circulation model

The atmospheric component of the fifth version of the Model for Interdisciplinary Research on Climate (MIROC; Watanabe et al., 2010) is based on a three-dimensional primitive equation in the hybrid σ–p coordinate, with a spectral truncation adopted for horizontal discretization. This study used the version labeled MIROC5-iso, in which water isotopes in the atmosphere and land surface parts were implemented by Okazaki and Yoshimura (2017, 2019). The resolution of the MIROC5-iso was set to a horizontal spectral truncation of T42 (approximately 280 km) and 40 vertical layers with coordinates. The detailed parameterizations of the models and its skills for the present-day climate conditions are discussed by Okazaki and Yoshimura (2017, 2019) and Kino et al. (2021).

2.2 Experimental design

Four experiments were performed using MIROC5-iso (Table S1). A pre-industrial (PI) simulation was set up following the "piControl" experimental design in the Coupled Model Intercomparison Project-Phase 6 (CMIP6; Eyring et al., 2016). The mean SST and SIC fields (monthly averaged over the period 1870 to 1899) were taken from the Atmospheric Modeling Intercomparison Project-Phase 2 (AMIP2; Taylor et al., 2000). Three LGM experiments were designed based on the PMIP4 protocol (Kageyama et al., 2017). For the elevation and distribution of ice sheets, the GLAC-1D reconstruction at the year 21 ka (Abe-Ouchi et al., 2013; Briggs et al., 2014; Tarasov and Peltier 2002; Tarasov et al., 2012; 2014) was used. The land-sea mask was extended according to the ice sheet. The boundary conditions of the land surface were the same as those in the PI simulation but masked by the LGM ice sheet. The $\delta^{18}O$ of seawater was set to a globally uniform value (+1 ‰), following Werner et al. (2018).

The LGM simulations differ in the provided sea surface boundary conditions (i.e., SST and SIC) to force MIROC5-iso. Two recent sets were used to investigate the influence of sea surface conditions on LGM $\delta^{18}O_p$ in Antarctica (Table S1). For LGM_G, the monthly SST and SIC data provided by the Glacial Ocean Map (GLOMAP; Paul et al., 2021) were used (Figure S1a). GLOMAP is a gridded LGM climatology reconstruction dataset based on faunal and floral assemblage data of the Multiproxy Approach for the Reconstruction of the Glacial Ocean Surface (MARGO) project and several estimates of the LGM SIC. GLOMAP dataset is known to have a larger cooling in the Southern Ocean compared to other datasets, as well as a more extended sea ice in this area. For LGM_M, SST and SIC simulated by Sherriff-Tadano et al. (accepted; hereafter, MIROC) were used (Figure S1b). The fourth generation of MIROC atmosphere-ocean coupled GCM successfully simulated the weak AMOC (Dome Fuji Ice Core Project Members, 2017; Obase et al., 2021) suggested by proxies. Sherriff-Tadano et al. (accepted) further improved expressions of mixed-phased clouds and reduced surface warm biases existed in the Southern Ocean. For detailed applications of MIROC5-iso, see Text S1.

In Figure 1a, SST in the southern hemisphere (SH) of LGM_G and LGM_M are presented as zonal mean anomalies compared to PI, as well as the LGM_G minus LGM_M difference. The sea ice of LGM_G expanded more than the one of LGM_M at every longitude (triangles in sub-figure a). The sensitivity experiment, LGM_Mw/Gice (i.e., MIROC SST and GLOMAP SIC), was conducted to linearly decompose the influences of SST and SIC that

differed for LGM_G and LGM_M. Therefore, LGM_G minus LGM_Mw/Gice (LGM_Mw/Gice minus LGM_M) indicates the individual influence of changes in SST (SIC).

2.3 Proxy data for model evaluation

Ten Antarctic ice core records were used for the evaluation (Table S2). For EDML, Dome B, Vostok, Dome C, Taylor Dome, Talos, WDC, and Byrd, $\Delta\delta^{18}O$ (Δ denotes climatological anomaly) for LGM minus PI in LGM compiled by Werner et al. (2018) was employed. For the South Pole, we used the result of $\Delta\delta^{18}O$ estimated by Steig et al. (2021).

For global evaluation, $\Delta\delta^{18}O$ data from speleothems (Comas-Bru et al., 2019, 2020) and ice cores (Kawamura et al., 2007; Landais et al., 2013; Uemura et al., 2018) are used to evaluate the simulated LGM climates globally. For speleothem, $\Delta\delta^{18}O$ in the calcite is obtained from the Speleothem Isotope Synthesis and Analysis version 2 (SISALv2) dataset (Comas-Bru et al., 2020). The speleothem values of $\Delta\delta^{18}O$ are converted in drip water as in Cauquoin et al. (2019), using the respective experiments and method of Tremaine et al. (2011).

2.4 Analysis method

Water isotope variables, such as $\delta^{18}O_p$, are always weighted using the amount of water (precipitation) because water isotopes are recorded in precipitation (Sime et al., 2008). Therefore, the climatological $\delta^{18}O_p$ is generally calculated as

$$\delta^{18}\mathrm{O_p} = \frac{\sum_t \left(\delta^{18}\mathrm{O}_{\mathrm{p},t} \times P_t\right)}{\sum_t P_t}$$

where P is precipitation and t the increase in time (in this study, t = 1 day). To investigate the contributions of daily atmospheric circulation and precipitation events on $\delta^{18}O_p$, we analyzed the climatological $\delta^{18}O_p$ without precipitation weighting (hereafter $\delta^{18}O_{pa}$), which is expressed as

$$\delta^{18}\mathrm{O_{pa}} = \frac{\sum_t \delta^{18}\mathrm{O}_{\mathrm{p},t}}{t_{max}}$$

where t_{max} is the number of the time steps.

3 Results

3.1 Evaluation of Last Glacial Maximum climate simulations in MIROC5-iso

First, we evaluated the modeled $\Delta\delta^{18}O_p$ by MIROC5-iso at global scale. The model-data comparison suggests that LGM_G is closer to the LGM proxies than LGM_M results (root mean square error RMSE = 2.39 and 3.37 ‰, respectively; see Figures S2b and S3b). The lower $\delta^{18}O_p$ values in our LGM simulations showed polar amplification in NH and SH (Figures S2a and S3a) as in certain previous studies (Cauquoin et al., 2019; Werner et al., 2001), which corresponds with surface cooling. The depletion in LGM_M was stronger in NH than in SH; $\Delta\delta^{18}O_p$ reached approximately −8 ‰ at 60°N and less than −2 ‰ at 60°S (Figure S3a). In contrast, depletion in the high latitudes of LGM_G was meridionally symmetrical: approximately −5 ‰ at 60°N and 60°S (Figure S2a).

We focus now on Antarctic region. We further evaluated the modeled $\Delta\delta^{18}O_p$ by MIROC5-iso (LGM_G and LGM_M minus PI in Figures 1b and 1c, respectively) using Antarctic ice core records. The red dots and line in Figures 1d show the model-data comparison at the 10 ice core locations and the associated linear fit, respectively. We found a better agreement with LGM_G minus PI results (a=1.08 and RMSE=3.361; a being the gradient of the linear regression line), although they overestimate the $\delta^{18}O_p$ decrease recorded in the ice cores, particularly in Taylor Dome and Talos (around -9.7 and -11.6 ‰, respectively). In the PI simulation, the elevations of Taylor and Talos Domes were lower than the real values (-885 and -1014 m, respectively; Table S2); therefore, excessively large elevation changes from PI to LGM may partly cause $\delta^{18}O_p$ change to be too large. The overestimated decrease in $\delta^{18}O_p$ over Antarctica may be due to the too low $\delta^{18}O_p$ at very low temperatures or high latitudes in MIROC5-iso (Figure S1b of Kino et al., 2021). We found a better estimation of $\Delta\delta^{18}O_p$ at a few sites in LGM_M minus PI results than in the LGM_G minus PI values (i.e., EDML, WDC, and Byrd). On the other hand, the $\Delta\delta^{18}O_p$ values of the East Antarctic sites were unrealistically diverse in LGM_M minus PI (Figure 1e). Therefore, the model-data was low (a=0.18 and RMSE=3.533; blue in Figure 1d) under this MIROC configuration.

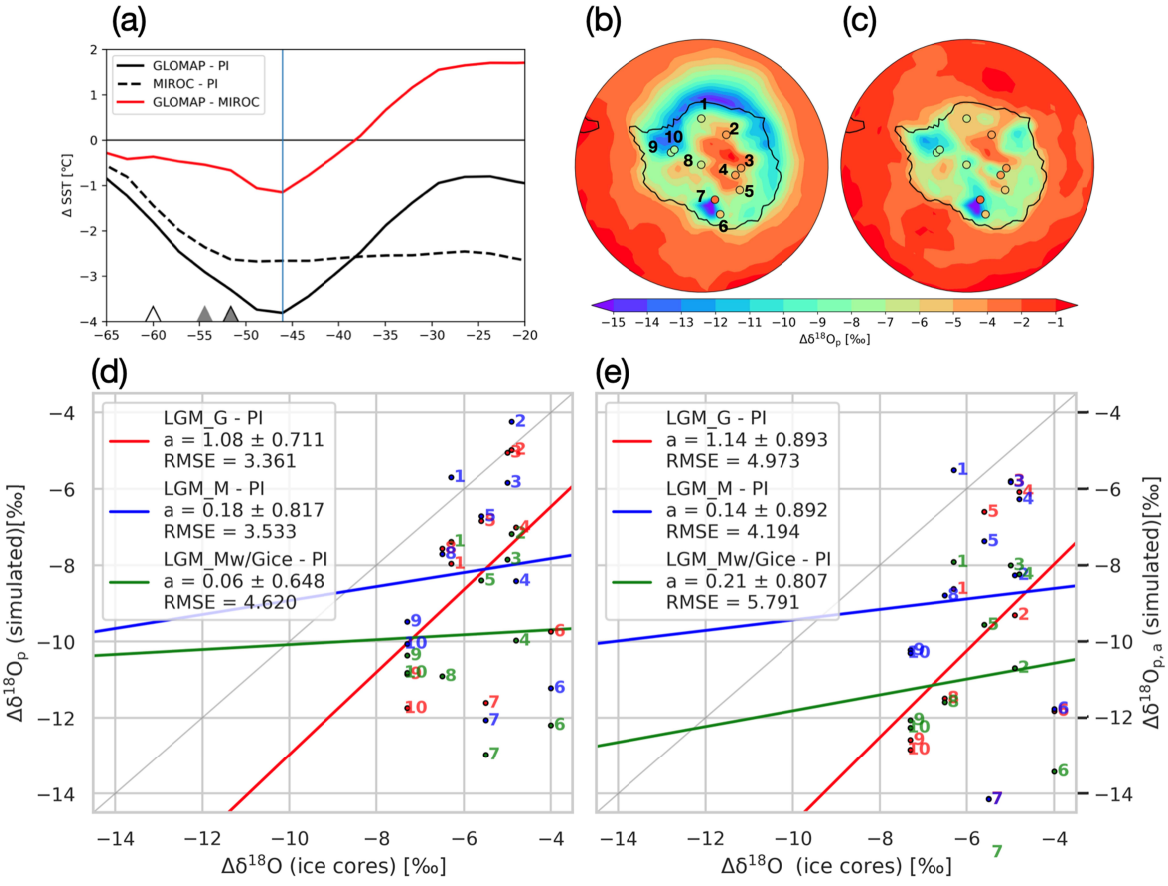

Figure 1. (a) Differences of zonal mean SST for LGM_G minus PI (solid black curve), LGM_M minus PI (dashed black curve), and LGM_G minus LGM_M (solid red curve). The zonal mean threshold of > 15 % of SIC in PI, LGM_G, and LGM_M are shown as white,

gray with black edge, and gray without edge triangles, respectively. The vertical blue line shows the zonal meant SST front of every experiment, which is entirely overlapping at 46.0°S. **(b)** and **(c)** Annual $\Delta\delta^{18}O_p$ for LGM_G minus PI and LGM_M minus PI, respectively; $\Delta\delta^{18}O_{ice\ cores}$ at different sites of Antarctic ice cores (Table S2). **(d)** and **(e)** $\Delta\delta^{18}O_{ice\ cores}$ vs. $\Delta\delta^{18}O_p$ and $\Delta\delta^{18}O_{pa}$ at different sites of Antarctic ice cores (Table S2) for LGM_G minus PI (red), LGM_M minus PI (blue), and LGM_Mw/Gice minus PI (green); the gradient of the linear regression fit (*a*) and the value of root mean square error (RMSE) are expressed in the legend panels.

In LGM_Mw/Gice minus PI, while the overestimation of the decrease in $\delta^{18}O_p$ was the strongest among our simulations, we found similar model-data linear regression slopes for $\Delta\delta^{18}O_p$ (a=0.06 and RMSE=4.620; the green line and dots in Figure 1b) than with LGM_M minus PI results. Therefore, we can conclude that LGM SST from GLOMAP yielded the optimal model-data agreement in LGM_G minus PI. Figure 2f also implies that $\delta^{18}O_p$ LGM decrease due to sea ice extension (from LGM_M to LGM_Mw/Gice) in almost the whole Antarctica was counter-balanced by SST substitution (from LGM_Mw/Gice to LGM_G; Figure 2c), particularly in East Antarctica.

The spatial features of the simulated LGM climates were preserved, regardless of the weighting by daily precipitation amounts. Figure 1e, using $\Delta\delta^{18}O_{pa}$ instead of $\Delta\delta^{18}O_p$ in the vertical axis, shows the systematic shifts toward lower $\Delta\delta^{18}O$ values compared to Figure 1c-1. This result suggests that the major factor underlying the varying $\Delta\delta^{18}O_p$ values among LGM experiments is not related to precipitation intermittency. It means that the general weakness of most climate models in reproducing Antarctic precipitation (Sime & Wolff, 2011) does not prevent to investigate the main controlling factors influencing the Antarctic $\Delta\delta^{18}O_p$ associated with change in SST. The oversight of daily precipitation weighting should induce apparent reduction, introducing different biases in the model experiments and between the polar ice core sites (Figures 1b–e). This would pose a critical issue in constraining the spatial and temporal relationship between $\Delta\delta^{18}O_p$ and ΔSAT, and so in reconstructing past temperature variations. It will be investigated in a future study.

4. Associations between Antarctic $\delta^{18}O_p$ and the Southern Atmospheric Mean States during Last Glacial Maximum

4.1. Decomposition of sea surface temperature and sea ice concentration effects

This section investigates the processes ruling $\delta^{18}O_p$ and $\delta^{18}O_{pa}$ values in Antarctica. As we confirmed that the daily precipitation weighting does not impact the basic distribution of $\Delta\delta^{18}O_p$ and $\Delta\delta^{18}O_{pa}$, we first described $\delta^{18}O_{pa}$ and then discussed the impact of daily precipitation weighting on $\delta^{18}O$.

The previous section showed that SST reconstruction from GLOMAP (LGM_G) gave a better model-data agreement compared to simulation results using MIROC SST (LGM_M). In this section, we analyze the LGM_G minus LGM_Mw/Gice to focus on the crucial processes relative to SST forcing only. In inland East Antarctica, $\delta^{18}O_{pa}$ increased by more than 1 ‰, particularly around Dome C, where it increased by more than 2 ‰ (Figure 2b). For the remaining region, $\delta^{18}O_{pa}$ decreased by approximately 1 ‰ in coastal West Antarctica (e.g., WDC). SST

substitution from GLOMAP to MIROC one does not impact $\delta^{18}O_{pa}$ in inland West Antarctica and around EDML. The slight decrease of $\delta^{18}O_{pa}$ in the western coast was attributed to the advection effect due the decrease in the sea-ice extent nearby. Over sea ice covered areas, $\delta^{18}O_{pa}$ decreased by 1–2 ‰ in the Atlantic and Indian Ocean sectors but only changed slightly in the Pacific sector. The ΔSAT around Dome C exceeded +1 °C and corresponded roughly to spatial variations of $\Delta\delta^{18}O_{pa}$ (Figure 2a). These spatial associations suggest that the same factors induce changes in SAT and $\delta^{18}O_{pa}$. Large-scale atmospheric circulation patterns in the southern mid-latitudes, such as the Southern Annular Mode (SAM) and the Pacific-South American (PSA) patterns, are well linked to the Antarctic surface climate (Marshall and Thompson, 2016).

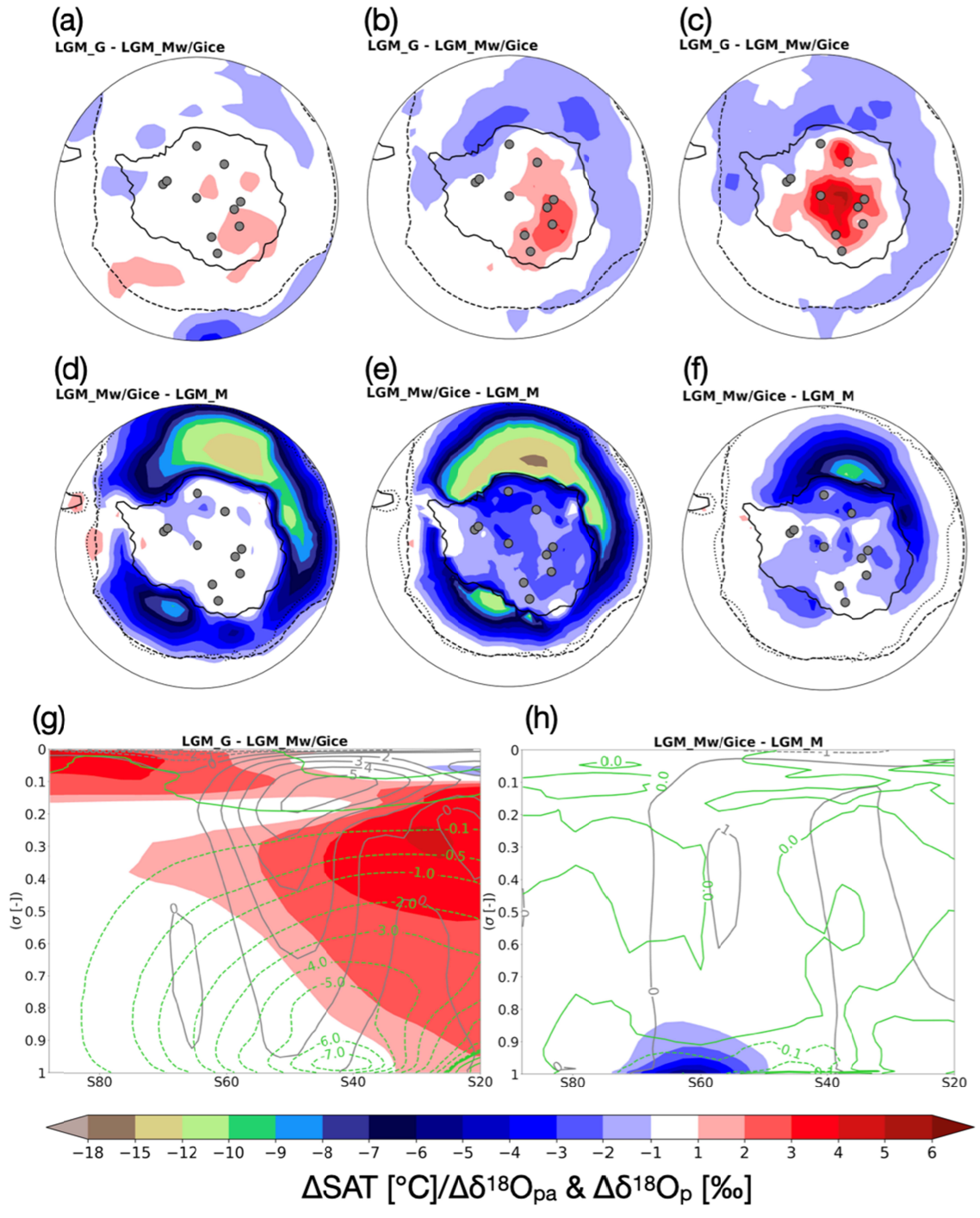

Figure 2. (a) Differences in annual mean climatological surface air temperature for LGM_G minus LGM_Mw/Gice. **(b)** Same as **(a)**, but for $\Delta\delta^{18}O_{pa}$. **(c)** Same as **(a)**, but for $\Delta\delta^{18}O_{p}$. **(d-f)**, Same as **(a-c)**, but for LGM_Mw/Gice minus LGM_M. **(e)** Zonal mean air temperature (shades), zonal wind (gray contours; m/s), and meridional vapor flux (green contours; g/kg•m/s) in the model vertical coordinates (values of 0 and 1 represent the top of the atmosphere and the surface, respectively). for LGM_G minus LGM_Mw/Gice. **(f)** Same as **(e)**, but for LGM_Mw/Gice minus LGM_M. For **(a-f)**, Antarctic ice core sites (Table S1) are shown as gray circles; 15 % of SIC are shown as solid (MIROC) and dashed (GLOMAP) contours.

The southern westerlies in LGM_G were enhanced 5 m/s in the upper troposphere compared to those in LGM_Mw/Gice (gray lines in Figure 2e). The steep meridional SST gradient in the southern mid-latitudes increased baroclinicity and storm track activities and strengthened the southern westerlies (Nakamura et al., 2008); LGM_G had a steeper SST gradient than LGM_Mw/Gice (red curve in Figure 1a). Sime et al. (2013) suggested that reducing the uncertainties of LGM SST are crucial for constraining southern westerlies. To summarize, the steep SST gradient in the southern mid-latitudes was the main cause of the strengthening of the southern westerlies in LGM_G (Figure S4a). The SST gradient in the sea-ice-free region was very similar in PI and LGM_Mw/Gice (0.91 and 0.91 °C/°, respectively), but was larger in LGM_G (1.04 °C/°). Consequently, the southern westerlies in LGM_G were strengthened and expanded southward (Figure S4a). In contrast, the southern westerlies in LGM_M and LGM_Mw/Gice changed little compared to the PI (Figures S4b–c). Although the southern westerlies in the MIROC5 series were further weak around 60°S compared to the observations (Watanabe et al., 2010), our results are consistent with the well-known dynamical atmosphere-ocean linkage in the southern mid-latitudes —intensified southern westerlies mitigate the meridional energy balance (Wunsch, 2003; Wyrwoll et al., 2000)— and other simulation studies (Nakamura et al., 2008; Ogawa et al., 2016; Sime et al., 2013).

The strengthened westerlies in LGM_G are associated with increased southward warm and humid air transportation. The shades and green contours in Figure 2e show the increase in air temperature and meridional vapor flux in the middle and upper troposphere south of 40°S, where SST decreased, as well as at lower latitudes (red curve in Figure 1a). Surface evaporation changed by the steepened meridional SST: it decreased with lower SST south of 40°S but increased with higher SST north of 40°S (Figure S5a). It suggests that the increase in evaporation in the relatively lower latitudes would move toward Antarctica and increase $\delta^{18}O_{pa}$ in inland Antarctica (Figure 2b).

Despite being a secondary factor, SICs significantly contributed to the differences between LGM_G and LGM_M (Figures 1b–e). We analyzed LGM_Mw/Gice minus LGM_M and confirmed the enhancement in isotopic fractionation processes during vapor transportation above the expanded sea ice. The sea ice extension altered the thermal interaction between the lower atmosphere and the sea surface. Also, it increased the surface albedo, which induced strong surface cooling and disruption of the supply of relatively heavy water isotopes from the sea surfaces, making lower $\delta^{18}O_{p}$ in the water vapor and precipitation. Cooling also enhances isotope fractionation processes as well (Lee et al., 2008) because the equilibrium isotope fractionations are relatively strong at relatively low temperatures (Yoshimura, 2015). Moreover,

kinetic fractionation occurs during condensation from vapor to ice under supersaturation conditions.

Our results are consistent with the ones from Lee et al. (2007; 2008) who pointed out the importance of evaporative recharge of water isotopes in vapor over the oceans and the rapid condensation of relatively heavy water isotopes in the air over sea ice, resulting in lower Antarctic water isotope ratios in precipitation. $\Delta^{18}O_{pa}$ in the Atlantic sector, where the sea ice expanded noticeably, decreased by more than 15 ‰ (Figure 2e) and was associated with cooling of more than 6 °C (Figure 2d). A larger extension of the sea ice cooled the lower atmosphere (shades in Figure 2f), too, while the associated changes in the southern westerlies and the meridional vapor transports were uncertain (gray and green contours in Figure 2f). The more extended sea ice in LGM_Mw/Gice did not change SAT over Antarctica (Figure 2d) but decreased $\delta^{18}O_{pa}$ by 1–3 and 1–2 ‰ in most of East and West Antarctica (Figure 2e), respectively. The non-associated responses of SAT and $\delta^{18}O_{pa}$ in Antarctica indicated that sea ice did not cool Antarctica directly but affected the vapor isotopic composition that was transported beyond the sea ice.

4.2. Contribution of the precipitation weighting effect, and combination of sea surface temperature and sea ice concentration effects

The daily precipitation weighting effect, which was reflected in $\delta^{18}O_p$ and not in $\delta^{18}O_{pa}$, changed the spatial features of $\Delta\delta^{18}O_p$ and $\Delta\delta^{18}O_{pa}$ over Antarctica for LGM_G minus LGM_Mw/Gice (steepened meridional SST gradient; Figures 2b–c). $\Delta\delta^{18}O_{pa}$ and ΔSAT (Figures 2a and c) increased around Dome C in East Antarctica, which spatially corresponds to an increase in precipitable water (vertically integrated atmospheric vapor amount; Figure S7a) associated with the enhanced warm and humid air inflows. So, the increase in $\Delta\delta^{18}O_p$ was stronger by 2–4 ‰ compared to $\Delta\delta^{18}O_{pa}$, especially in inland Antarctica (Figures 2b and 2c). It suggests that daily $\delta^{18}O_p^t$ is associated with precipitation intermittency, especially in inland Antarctica. The large discrepancy of $\Delta\delta^{18}O_p$ and $\Delta\delta^{18}O_{pa}$ at the South Pole (+3.3 ‰; Figures 2b–c) typically reflected less precipitation inland compared to the coastal area.

For LGM_Mw/Gice minus LGM_M (sea ice expansion), the differences between $\Delta\delta^{18}O_p$ and $\Delta\delta^{18}O_{pa}$ over Antarctica were spatially uniform (Figures 2e–f). The $\Delta\delta^{18}O_p$ were approximately 1 ‰ higher than $\Delta\delta^{18}O_{pa}$ in East Antarctica. The results suggested that the sea ice expansion influenced the mean fields, but not the precipitation intermittency. It was consistent with the absence of enhancement of the warm and humid air inflows, associated with unclear changes in the atmospheric zonal fields in the mid-latitudes and precipitable water and ΔSAT over Antarctica (Figures 2f, S7b, and 2d).

Finally, in most of East Antarctica (except for EDML), the increase and decrease in $\delta^{18}O_{pa}$ induced by both SST and SIC substitution resulted in little changes only (Figure S6b), suggesting that SST and SIC impacts would compensate each other. The opposite is true for West Antarctica, around EDML and at west of Dome Fuji. $\Delta\delta^{18}O_{pa}$ decreased (Figure S6b) due to SIC effects (Figure 2e) and the precipitation weighting effect induced higher $\Delta\delta^{18}O_{pa}$ compared to $\Delta\delta^{18}O_p$ over Antarctica and surrounding sea ice regions (Figures S7b–c). The spatial heterogeneity of the changes in $\delta^{18}O_p$, particularly owing to SST differences between GLOMAP and MIROC, resulted in significantly different model-data agreements (Figures 1b–e).

5 Discussion and Conclusions

This study investigated the role of atmospheric circulation in the southern mid-latitudes in determining $\delta^{18}O_p$ during the LGM in Antarctica, especially in the eastern part, in relation with SST and SIC conditions in SH. Figure 3 illustrates the main findings of our study. Our three LGM experiments showed that the steep meridional SST gradient strengthened the southern westerlies, enhancing southward humid and warm air fluxes from lower latitudes to the Antarctic continent. It resulted relatively high $\delta^{18}O_p$ in inland East Antarctica (orange legends in Figure 3). This process is associated with blocking events (Dittman et al., 2016; Hirasawa et al., 2000; 2013; Schlosser et al., 2017) and SAM (Kino et al., 2021; Noone & Simmonds, 2002). The precipitation weighting effect on $\Delta\delta^{18}O_p$ distribution was secondary but cannot be disregarded for a better quantitative determination. In other words, a better representation of Antarctic precipitation in climate models is required to improve the isotopic model-data agreement.

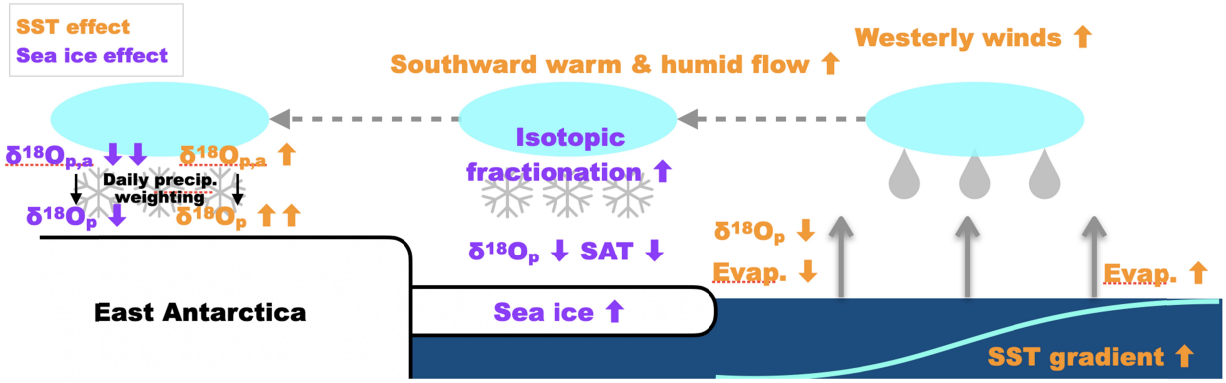

Figure 3. Schematic view of the processes ruling the $\Delta\delta^{18}O_p$ in inland East Antarctica during LGM. The orange and purple colors represent the key processes associated with the substitution of SST (LGM_G minus LGM_Mw/Gice) and SIC (LGM_Mw/Gice minus LGM_M) fields, respectively. The upward and downward arrows represent the increases and decreases of the variables, respectively.

The association between water isotopic signals in Antarctic ice cores and SST in the Southern Ocean has been considered in the reconstruction of past Antarctic temperature changes in ice cores (Uemura et al., 2018). While the authors assumed a one-dimensional Lagrangian transportation from sea surface to inland Antarctica, this study used a complex climate model to explicitly simulate global three-dimensional atmospheric circulation. Our simulation supported this concept of SST – $\delta^{18}O_p$ association in inland East Antarctica, even when considering daily precipitation events owing to synoptic-scale atmospheric circulation. Further analyses of secondary ordered water isotopes (i.e., d-excess) to connect Rayleigh model-based and GCM-based studies are required. Conducting water-tagging experiments to find moisture sources is within the scope of future studies.

We also confirmed that the influence of sea ice expansion in SH was of the same order as the influence of the changes in the southern westerlies associated with steep meridional SST gradient. Sea ice expansion radically reduced the $\delta^{18}O_p$ over sea ice covered areas and affected the $\delta^{18}O_p$ over Antarctica, as suggested by Lee et al. (2008; magenta legends in Figure 3). As a

novelty of this study, we showed that the low $\delta^{18}O_{pa}$ over Antarctica due to greater sea ice expansion would not be associated with large-scale atmospheric circulations (as in the case in SST substitution). Therefore, precipitation weighting mitigated the decrease in $\delta^{18}O_p$ over Antarctica. As a result, $\Delta\delta^{18}O_p$ in East Antarctica was dominated by SST substitution and the associated changes in the southern westerlies, even though the influences of SST and sea ice substitution on $\Delta\delta^{18}O_{pa}$ were of the same order. We cannot exclude the model dependency of our results. So, comparisons among multiple isotope-enabled climate models, including Antarctic precipitation, are required for further investigation. Our study did not remove the biases and uncertainties inherent in the AGCM of the MIROC series. Nevertheless, the use of different sea surface boundary conditions with different characteristics allowed us to investigate the impacts of the southern westerlies on the $\delta^{18}O_p$ over Antarctica.

Our results imply that the southern westerlies are important mediators between the sea surface and $\delta^{18}O$ in ice cores. Ice cores would play crucial roles in constraining past southern westerlies, the features of which are discussed for the LGM period (Kohfeld et al., 2013; Sime et al., 2013; Sime et al., 2016). So, isotope climate models that can simulate three-dimensional atmospheric circulation have the potential to play an even more important role in Antarctic ice core research.

Acknowledgments

- The first author was supported by the Japan Society for the Promotion of Science (JSPS) via a Grant-in-Aid for JSPS Fellows.
- This work was supported by the Japan Society for the Promotion of Science (JSPS) via Grants-in-Aid 17K14397, 19J14488, 21H05002, 22K21323, and JRPs-LEAD with DFG via 416767181, and the Integrated Research Program for Advancing Climate Models (TOUGOU; JPMXD0717935457), ArCS II (JP-MXD1420318865), DIAS (JPMXD0716808979), and the advanced studies of climate change projection (SENTAN; JPMXD0722680395) from the Ministry of Education, Culture, Sports, Science and Technology (MEXT), Japan, and the Environment Research and Technology Development Fund S-20 (Grant Number JPMEERF21S12020) from the Environmental Restoration and Conservation Agency of Japan.

- We also thank Masakazu Yoshimori, Yukari Takayabu, Masahiro Watanabe, Hisashi Nakamura, Yukio Masumoto, Masahide Kimoto, and Fumiaki Ogawa for their constructive comments.

Open Research

- Ice core data used for Figures S2 and S3 are available at https://www.ncdc.noaa.gov/data-access/paleoclimatology-data and are reported in Cauquoin et al. (2019). Ice core data used for Figure 1, except for the South Pole, are available at Table 1 of Werner et al. (2018). For the South Pole, data is available at https://www.usap-dc.org/view/dataset/601239. SISAL speleothem dataset from Comas-Bru et al. (2020) is available at https://researchdata.reading.ac.uk/256/. The GLOMAP from Paul et al. (2022) is available at https://doi.pangaea.de/10.1594/PANGAEA.923262. The SST and SIC outputs from MIROC4m-AOGCM is available from the authors of Sherriff-Tadano et al. (accepted).

- The code of the isotopic version MIROC5-iso is available upon request on the IIS's GitLab repository (http://isotope.iis.u-tokyo.ac.jp:8000/gitlab/miroc-iso/miroc5-iso, Okazaki and Yoshimura, 2019).
- The source codes and data used in this study are available at https://github.com/kanonundgigue/kino2023grl and https://doi.org/10.5281/zenodo.7582876.

References

Ayako Abe-Ouchi, F. Saito, K. Kawamura, M. Raymo, J. Okuno, K. Takahashi, and H. Blatter: Insolation-driven 100,000-year glacial cycles and hysteresis of ice-sheet volume, Nature, 500, 190–193, 2013, doi:10.1038/nature12374

Atsawawaranunt, K., Harrison, S., & Comas-Bru, L. (2019). SISAL (Speleothem Isotopes Synthesis and AnaLysis Working Group) database version 1b [Data set]. University of Reading. https://doi.org/10.17864/1947.189>

Augustin, L., Barbante, C., Barnes, P. R. F., Barnola, J. M., Bigler, M., Castellano, E., et al. (2004). Eight glacial cycles from an Antarctic ice core. *Nature*, *429*(6992), 623–628. https://doi.org/10.1038/nature02599

Braconnot, P., Albani, S., Balkanski, Y., Cozic, A., Kageyama, M., Sima, A., et al. (2021). Impact of dust in PMIP-CMIP6 mid-Holocene simulations with the IPSL model. *Climate of the Past*, *17*(3), 1091–1117. https://doi.org/10.5194/cp-17-1091-2021

Briggs, R. D., Pollard, D., & Tarasov, L. (2014). A data-constrained large ensemble analysis of Antarctic evolution since the Eemian. *Quaternary Science Reviews*, *103*, 91–115. https://doi.org/10.1016/j.quascirev.2014.09.003

Buizert, C., Gkinis, V., Severinghaus, J. P., He, F., Lecavalier, B. S., Kindler, P., et al. (2014). Greenland temperature response to climate forcing during the last deglaciation. *Science*, *345*(6201), 1177–1180. https://doi.org/10.1126/science.1254961

Buizert, C., Fudge, T. J., Roberts, W. H. G., Steig, E. J., Sherriff-Tadano, S., Ritz, C., et al. (2021). Antarctic surface temperature and elevation during the Last Glacial Maximum. *Science*, *372*(6546), 1097–1101. https://doi.org/10.1126/science.abd2897

443 Cauquoin, A., Landais, A., Raisbeck, G. M., Jouzel, J., Bazin, L., Kageyama, M., et al. (2015).
444 Comparing past accumulation rate reconstructions in East Antarctic ice cores using 10Be,
445 water isotopes and CMIP5-PMIP3 models. *Climate of the Past*, *11*(3), 355–367.
446 https://doi.org/10.5194/cp-11-355-2015
447 Cauquoin, A., Risi, C., & Vignon, É. (2019). Importance of the advection scheme for the
448 simulation of water isotopes over Antarctica by atmospheric general circulation models: A
449 case study for present-day and Last Glacial Maximum with LMDZ-iso. *Earth and*
450 *Planetary Science Letters*, *524*, 115731. https://doi.org/10.1016/j.epsl.2019.115731
451 Cauquoin, A., Werner, M., & Lohmann, G. (2019). Water isotopes – climate relationships for the
452 mid-Holocene and preindustrial period simulated with an isotope-enabled version of MPI-
453 ESM. Climate of the Past, 15(6), 1913–1937. https://doi.org/10.5194/cp-15-1913-2019
454 Comas-Bru, L., Harrison, S. P., Werner, M., Rehfeld, K., Scroxton, N., Veiga-Pires, C., &
455 SISAL working group members. (2019). Evaluating model outputs using integrated global
456 speleothem records of climate change since the last glacial. Climate of the Past, 15(4),
457 1557–1579. https://doi.org/10.5194/cp-15-1557-2019
458 Comas-Bru, L., Rehfeld, K., Roesch, C., Amirnezhad-Mozhdehi, S., Harrison, S. P.,
459 Atsawawaranunt, K., et al. (2020). SISALv2: A comprehensive speleothem isotope
460 database with multiple age-depth models. Earth System Science Data Discussions, 1–47.
461 https://doi.org/10.5194/essd-2020-39
462 Dahe, Q., Petit, J. R., Jouzel, J., & Stievenard, M. (1994). Distribution of stable isotopes in
463 surface snow along the route of the 1990 International Trans-Antarctica Expedition.
464 *Journal of Glaciology*, *40*(134), 107–118. https://doi.org/10.3189/S0022143000003865

Dansgaard, W. (1964). Stable isotopes in precipitation. *Tell'Us*, *16*(4), 436–468. https://doi.org/10.3402/tellusa.v16i4.8993

Dittmann, A., Schlosser, E., Masson-Delmotte, V., Powers, J. G., Manning, K. W., Werner, M., & Fujita, K. (2016). Precipitation regime and stable isotopes at Dome Fuji, East Antarctica. *Atmospheric Chemistry and Physics*, *16*(11), 6883–6900. https://doi.org/10.5194/acp-16-6883-2016

Dome Fuji Ice Core Project Members. (2017). State dependence of climatic instability over the past 720,000 years from Antarctic ice cores and climate modeling. *Science Advances*, *3*(2), e1600446.

Eyring, V., Bony, S., Meehl, G. A., Senior, C. A., Stevens, B., Stouffer, R. J., & Taylor, K. E. (2016). Overview of the Coupled Model Intercomparison Project Phase 6 (CMIP6) experimental design and organization. *Geoscientific Model Development*, *9*(5), 1937–1958. https://doi.org/10.5194/gmd-9-1937-2016

Fujita, K., & Abe, O. (2006). Stable isotopes in daily precipitation at Dome Fuji, East Antarctica. *Geophysical Research Letters*, *33*(18). https://doi.org/10.1029/2006gl026936

Hirasawa, N., Nakamura, H., & Yamanouchi, T. (2000). Abrupt changes in meteorological conditions observed at an inland Antarctic Station in association with wintertime blocking. *Geophysical Research Letters*, *27*(13), 1911–1914. https://doi.org/10.1029/1999gl011039

Hirasawa, N., Nakamura, H., Motoyama, H., Hayashi, M., & Yamanouchi, T. (2013). The role of synoptic-scale features and advection in prolonged warming and generation of different forms of precipitation at Dome Fuji station, Antarctica, following a prominent blocking event. *Journal of Geophysical Research*, *118*(13), 6916–6928. https://doi.org/10.1002/jgrd.50532

Ivanovic, Gregoire, Kageyama, Roche, Valdes, Burke, et al. (2016). Transient climate simulations of the deglaciation 21–9 thousand years before present (version 1) – PMIP4 Core experiment design and boundary conditions. *Geoscientific Model Development*, *9*(7), 2563–2587.

Joussaume, S., & Taylor, K. E. (2021). PMIP: Looking back to its first phase (Vol. 29, pp. 64–65). Past Global Changes (PAGES). https://doi.org/10.22498/pages.29.2.64

Jouzel, J., Russell, G. L., Suozzo, R. J., Koster, R. D., White, J. W. C., & Broecker, W. S. (1987). Simulations of the HDO and H218O atmospheric cycles using the NASA GISS general circulation model: The seasonal cycle for present-day conditions. *Journal of Geophysical Research*, *92*(D12), 14739. https://doi.org/10.1029/jd092id12p14739

Kageyama, M., Albani, S., Braconnot, P., Harrison, S. P., Hopcroft, P. O., Ivanovic, R. F., et al. (2017). The PMIP4 contribution to CMIP6 – Part 4: Scientific objectives and experimental design of the PMIP4-CMIP6 Last Glacial Maximum experiments and PMIP4 sensitivity experiments. *Geosci. Model Dev.*, *10*(11), 4035–4055.

Kageyama, M., Abe-Ouchi, A., Obase, T., Ramstein, G., & Valdes, P. J. (2021). Modeling the climate of the last glacial maximum from PMIP1 to PMIP4. In P. B. A. K. J. M. Paul J. Valdes (Ed.) (Vol. 29, pp. 80–81). Past Global Changes (PAGES). https://doi.org/10.22498/pages.29.2.80

Kawamura, K., Parrenin, F., Lisiecki, L., Uemura, R., Vimeux, F., Severinghaus, J. P., et al. (2007). Northern Hemisphere forcing of climatic cycles in Antarctica over the past 360,000 years. Nature, 448(7156), 912–916. https://doi.org/10.1038/nature06015

Kino, K., Okazaki, A., Cauquoin, A., & Yoshimura, K. (2021). Contribution of the southern annular mode to variations in water isotopes of daily precipitation at dome Fuji, east

511 Antarctica. *Journal of Geophysical Research*, *126*(23).
512 https://doi.org/10.1029/2021jd035397
513 Kohfeld, K. E., Graham, R. M., de Boer, A. M., Sime, L. C., Wolff, E. W., Le Quéré, C., &
514 Bopp, L. (2013). Southern Hemisphere westerly wind changes during the Last Glacial
515 Maximum: paleo-data synthesis. *Quaternary Science Reviews*, *68*, 76–95.
516 https://doi.org/10.1016/j.quascirev.2013.01.017
517 Krinner, G., & Werner, M. (2003). Impact of precipitation seasonality changes on isotopic
518 signals in polar ice cores: a multi-model analysis. *Earth and Planetary Science Letters*,
519 *216*(4), 525–538. https://doi.org/10.1016/S0012-821X(03)00550-8
520 Landais, A., Dreyfus, G., Capron, E., Jouzel, J., Masson-Delmotte, V., Roche, D. M., et al.
521 (2013). Two-phase change in CO2, Antarctic temperature and global climate during
522 Termination II. Nature Geoscience, 6(12), 1062–1065. https://doi.org/10.1038/ngeo1985
523 Lee, J.-E., Fung, I., DePaolo, D. J., & Otto-Bliesner, B. (2008). Water isotopes during the Last
524 Glacial Maximum: New general circulation model calculations. *Journal of Geophysical*
525 *Research*, *113*(D19), 1341. https://doi.org/10.1029/2008jd009859
526 Lorius, & Merlivat. (1977). Distribution of mean surface stable isotope values in East Antarctica,
527 Isotopes and Impurities in Snow and Ice. *International Association of Hydrological*
528 *Sciences, Publication*, *118*, 127–137.
529 Lorius, C., Merlivat, L., Jouzel, J., & Pourchet, M. (1979). A 30,000-yr isotope climatic record
530 from Antarctic ice. *Nature*, *280*(5724), 644–648. https://doi.org/10.1038/280644a0
531 Marshall, G. J., & Thompson, D. W. J. (2016). The signatures of large-scale patterns of
532 atmospheric variability in Antarctic surface temperatures. *Journal of Geophysical*
533 *Research*, *121*(7), 3276–3289. https://doi.org/10.1002/2015jd024665

534 Marshall, G. J., Thompson, D. W. J., & van den Broeke, M. R. (2017). The Signature of
535 Southern Hemisphere Atmospheric Circulation Patterns in Antarctic Precipitation.
536 *Geophysical Research Letters*, *44*(22), 11580–11589.
537 https://doi.org/10.1002/2017GL075998
538 McManus, J. F., Francois, R., Gherardi, J.-M., Keigwin, L. D., & Brown-Leger, S. (2004).
539 Collapse and rapid resumption of Atlantic meridional circulation linked to deglacial climate
540 changes. *Nature*, *428*(6985), 834–837. https://doi.org/10.1038/nature02494
541 Motoyama, H. (2005). Seasonal variations in oxygen isotope ratios of daily collected
542 precipitation and wind drift samples and in the final snow cover at Dome Fuji Station,
543 Antarctica. *Journal of Geophysical Research*, *110*(D11).
544 https://doi.org/10.1029/2004jd004953
545 Nakamura, H., Sampe, T., Goto, A., Ohfuchi, W., & Xie, S.-P. (2008). On the importance of
546 midlatitude oceanic frontal zones for the mean state and dominant variability in the
547 tropospheric circulation. *Geophysical Research Letters*, *35*(15).
548 https://doi.org/10.1029/2008gl034010
549 Noone, D., & Simmonds, I. (2002). Annular variations in moisture transport mechanisms and the
550 abundance of δ18O in Antarctic snow. *Journal of Geophysical Research*, *107*(D24), 4742.
551 https://doi.org/10.1029/2002JD002262
552 Ogawa, F., Nakamura, H., Nishii, K., Miyasaka, T., & Kuwano-Yoshida, A. (2016). Importance
553 of Midlatitude Oceanic Frontal Zones for the Annular Mode Variability: Interbasin
554 Differences in the Southern Annular Mode Signature. *Journal of Climate*, *29*(17), 6179–
555 6199. https://doi.org/10.1175/JCLI-D-15-0885.1

Okazaki, A., & Yoshimura, K. (2017). Development and evaluation of a system of proxy data assimilation for paleoclimate reconstruction. *Climate of the Past*, *13*(4), 379–393. https://doi.org/10.5194/cp-13-379-2017

Okazaki, A., & Yoshimura, K. (2019). Global evaluation of proxy system models for stable water isotopes with realistic atmospheric forcing. *Journal of Geophysical Research*, *124*(16), 8972–8993. https://doi.org/10.1029/2018jd029463

Paul, A., Mulitza, S., Stein, R., & Werner, M. (2021). A global climatology of the ocean surface during the Last Glacial Maximum mapped on a regular grid (GLOMAP). *Climate of the Past*, *17*(2), 805–824. https://doi.org/10.5194/cp-17-805-2021

Satow, K., Watanabe, O., Shoji, H., & Motoyama, H. (1999). The relationship among accumulation rate, stable isotope ratio and surface temperature on the plateau of east Dronning Maud Land, Antarctica. *Polar Meteorology and Glaciology*, *13*, 43–52. https://doi.org/10.15094/00002888

Schlosser, E., Manning, K. W., Powers, J. G., Duda, M. G., Birnbaum, G., & Fujita, K. (2010). Characteristics of high-precipitation events in Dronning Maud Land, Antarctica. *Journal of Geophysical Research*, *115*(D14), 3518. https://doi.org/10.1029/2009JD013410

Schlosser, E., Dittmann, A., Stenni, B., Powers, J. G., Manning, K. W., Masson-Delmotte, V., et al. (2017). The influence of the synoptic regime on stable water isotopes in precipitation at Dome C, East Antarctica. *The Cryosphere*, *11*(5), 2345–2361. https://doi.org/10.5194/tc-11-2345-2017

Sherriff-Tadano, S., & Klockmann, M. (2021). PMIP contributions to understanding the deep ocean circulation of the Last Glacial Maximum. *Past Global Change Magazine*, *29*(2), 84–85. https://doi.org/10.22498/pages.29.2.84

579 Sherriff-Tadano, S., Abe-Ouchi, A., Yoshimori, M., Hotta, H., Kikuchi, M., Ohgaito, R., et al.
580 (accepted). Southern Ocean surface temperatures and cloud biases in climate models
581 connected to the representation of glacial deep ocean circulation. *Journal of Climate*
582 Sime, L. C., & Wolff, E. W. (2011, November 9). Antarctic accumulation seasonality. *Nature*.
583 https://doi.org/10.1038/nature10613
584 Sime, L. C., Tindall, J. C., Wolff, E. W., Connolley, W. M., & Valdes, P. J. (2008). Antarctic
585 isotopic thermometer during a CO2forced warming event. *Journal of Geophysical*
586 *Research*, *113*(D24), D06107. https://doi.org/10.1029/2008jd010395
587 Sime, L. C., Wolff, E. W., Oliver, K. I. C., & Tindall, J. C. (2009). Evidence for warmer
588 interglacials in East Antarctic ice cores. *Nature*, *462*(7271), 342–345.
589 https://doi.org/10.1038/nature08564
590 Sime, L. C., Kohfeld, K. E., Le Quéré, C., Wolff, E. W., de Boer, A. M., Graham, R. M., &
591 Bopp, L. (2013). Southern Hemisphere westerly wind changes during the Last Glacial
592 Maximum: model-data comparison. *Quaternary Science Reviews*, *64*, 104–120.
593 https://doi.org/10.1016/j.quascirev.2012.12.008
594 Sime, L. S., Hodgson, D., Bracegirdle, T. J., Allen, C., Perren, B., Roberts, S., & de Boer, A. M.
595 (2016). Sea ice led to poleward-shifted winds at the Last Glacial Maximum: the influence
596 of state dependency on CMIP5 and PMIP3 models. *Climate of the Past*, *12*(12), 2241–
597 2253. https://doi.org/10.5194/cp-12-2241-2016>
598 Steig, E. J., Jones, T. R., Schauer, A. J., Kahle, E. C., Morris, V. A., Vaughn, B. H., et al. (2021).
599 Continuous-Flow Analysis of δ17O, δ18O, and δD of H2O on an Ice Core from the South
600 Pole. *Frontiers of Earth Science in China*, *9*, 72. https://doi.org/10.3389/feart.2021.640292

601 Stenni, B., Scarchilli, C., Masson-Delmotte, V., Schlosser, E., Ciardini, V., Dreossi, G., et al.
602 (2016). Three-year monitoring of stable isotopes of precipitation at Concordia Station, East
603 Antarctica. *The Cryosphere*, *10*(5), 2415–2428. https://doi.org/10.5194/tc-10-2415-2016
604 Lev Tarasov and W. Richard Peltier Greenland glacial history and local geodynamic
605 consequences, Geophysical Journal International, 150, July 2002, Pages 198-
606 229, doi:10.1046/j.1365-246X.2002.01702.x
607 Tarasov, L., Dyke, A. S., Neal, R. M., & Peltier, W. R. (2012). A data-calibrated distribution of
608 deglacial chronologies for the North American ice complex from glaciological modeling.
609 *Earth and Planetary Science Letters*, *315-316*, 30–40.
610 https://doi.org/10.1016/j.epsl.2011.09.010
611 Lev Tarasov, Anna Hughes, Richard Gyllencreutz, Oystein Strand Lohne, Jan Mangerud and
612 John-Inge Svendsen, The global GLAC-1c deglaciation chronology, melwater pulse 1-a,
613 and a question of missing ice, IGS Symposium on Contribution of Glaciers and Ice Sheets
614 to Sea-Level Change, 2014
615 Taylor, K. E., Williamson, D., & Zwiers, F. (2000). *The sea surface temperature and sea-ice*
616 *concentration boundary conditions for AMIP II simulations*. Program for Climate Model
617 Diagnosis and Intercomparison, Lawrence River. Retrieved from
618 https://pcmdi.llnl.gov/report/pdf/60.pdf?id=16
619 Tremaine, D. M., Froelich, P. N., & Wang, Y. (2011). Speleothem calcite farmed in situ: Modern
620 calibration of δ18O and δ13C paleoclimate proxies in a continuously-monitored natural
621 cave system. Geochimica et Cosmochimica Acta, 75(17), 4929–4950.
622 https://doi.org/10.1016/j.gca.2011.06.005

Turner, J., Phillips, T., Thamban, M., Rahaman, W., Marshall, G. J., Wille, J. D., et al. (2019). The dominant role of extreme precipitation events in antarctic snowfall variability. *Geophysical Research Letters*, *46*(6), 3502–3511. https://doi.org/10.1029/2018gl081517

Uemura, R., Motoyama, H., Masson-Delmotte, V., Jouzel, J., Kawamura, K., Goto-Azuma, K., et al. (2018). Asynchrony between Antarctic temperature and CO2 associated with obliquity over the past 720,000 years. *Nature Communications*, *9*(1), 961. https://doi.org/10.1038/s41467-018-03328-3

Watanabe, M., Suzuki, T., O'ishi, R., Komuro, Y., Watanabe, S., Emori, S., et al. (2010). Improved Climate Simulation by MIROC5: Mean States, Variability, and Climate Sensitivity. *Journal of Climate*, *23*(23), 6312–6335. https://doi.org/10.1175/2010JCLI3679.1

Werner, Haese, Xu, Zhang, Butzin, & Lohmann. (2016). Glacial--interglacial changes in H218O, HDO and deuterium excess -- results from the fully coupled ECHAM5/MPI-OM Earth system model. *Geoscientific Model Development*, *9*(2), 647–670.

Werner, M., Heimann, M., & Hoffmann, G. (2001). Isotopic composition and origin of polar precipitation in present and glacial climate simulations. *Tellus. Series B, Chemical and Physical Meteorology*, *53*(1), 53–71. https://doi.org/10.3402/tellusb.v53i1.16539

Werner, M., Jouzel, J., Masson-Delmotte, V., & Lohmann, G. (2018). Reconciling glacial Antarctic water stable isotopes with ice sheet topography and the isotopic paleothermometer. *Nature Communications*, *9*(1), 3537. https://doi.org/10.1038/s41467-018-05430-y

644 Wunsch, C. (2003). Determining paleoceanographic circulations, with emphasis on the Last
645 Glacial Maximum. *Quaternary Science Reviews*, *22*(2), 371–385.
646 https://doi.org/10.1016/S0277-3791(02)00177-4
647 Wyrwoll, K.-H., Dong, B., & Valdes, P. (2000). On the position of southern hemisphere
648 westerlies at the Last Glacial Maximum: an outline of AGCM simulation results and
649 evaluation of their implications. *Quaternary Science Reviews*, *19*(9), 881–898.
650 https://doi.org/10.1016/S0277-3791(99)00047-5